6th European Conference on Computational Mechanics (ECCM 6)
7th European Conference on Computational Fluid Dynamics (ECFD 7)
1115 June 2018, Glasgow, UK

HEAT TRANSFER MAXIMIZATION IN A THREE DIMENSIONAL CONDUCTIVE DIFFERENTIALLY HEATED CAVITY BY MEANS OF TOPOLOGY OPTIMIZATION

CLIO SAGLIETTI[1], EDDIE WADBRO[2], MARTIN BERGGREN[2] AND DAN S. HENNINGSON[1]

[1] Linné FLOW Centre and Swedish e-Science Research Centre (SeRC), KTH Mechanics
Royal Institute of Technology
SE-114 28 Stockholm, Sweden
clios@mech.kth.se
henning@mech.kth.se

[2] Department of Computing Science, Umeå University
SE-901 87 Umeå, Sweden
eddie.wadbro@umu.se
martin.berggren@cs.umu.se

Key words: Topology optimization; Conjugate heat transfer; Three dimensional conductive differentially heated cavity; Natural convection; Heat sinks.

Abstract. The thermal performance of heat sinks is enhanced, in the present paper, by applying a material distribution topology optimization approach. We consider solid structures enclosed in three dimensional steady-state conductive differentially heated cavities. The algorithm iteratively updates the geometry of a heat sink, relying on gradient information. The gradient information are computed using adjoint sensitivity methods, combined with high-order accuracy direct numerical simulations. A complete conjugated problem is solved, in which we describe the effect of the solid material on the surrounding flow through the action of a Brinkman friction term in the Navier–Stokes equations, and we map the material distribution function onto the thermal conductivity and heat capacity in the energy conservation equation. Additionally, advanced filtering techniques are applied for enforcing a desired length scale to the solid structure. The success of the method is presented with a thorough physical investigation of the optimal results, which deliver a substantial increase of the heat transfer.

1 INTRODUCTION

Optimization of natural convection cooling systems is a major engineering challenge of the present times. Because of their high reliability and durability, they can be employed for many industrial applications. One of the most advanced techniques for optimizing such systems is to act on the topology of the heat sink, that is, how its geometry is connected,

thus optimizing the thermal performance by canalizing the surrounding flow. Bendsøe and Kikuchi[1] introduced a method for optimization of load carrying elastic structures that has become influential also for other applications,[2] the material distribution topology optimization method. This approach aims to optimally distribute in space a composite material function. Each point of the domain is a degree of freedom, thus there are no *a priori* restriction on the optimal topology.

Optimization of simple conduction problems was the first form of topology optimization for enhancing thermal performances.[2] In the following years, more advanced studies have included convection contributions. At the beginning, convective effects were just treated as a boundary condition;[3] later, the entire conjugate heat transfer has been considered. The first attempts were limited to Stokes problems,[4,5] but more recently, the feasibility of the method has been proven on Navier–Stokes problems.[6–8] There are various ways of describing the embedded heat sink. One way is to use a level set function,[9,10] another is the immersed boundary method.[11] In the second case, the momentum conservation law is solved in the whole domain, but the velocity is penalized inside the solid structure using a Brinkman friction term.[12] Moreover, the material distribution function is also mapped to the thermal properties in solving the energy conservation law.[13]

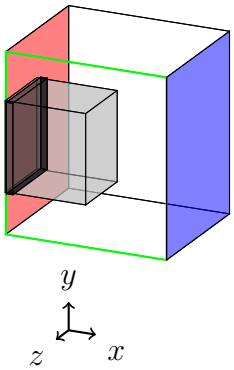

Figure 1: Sketch of the computational domain (Ω: $-0.5 \leq x \leq 0.5$, $-0.5 \leq y \leq 0.5$, and $-0.5 \leq z \leq 0$) and of the optimization domain (in gray Ω_O: $-0.46 \leq x \leq -0.25$, $-0.25 \leq y \leq 0.25$, and $-0.25 \leq z \leq 0$). On the cold wall, Γ_1 (in blue), the objective function $\mathscr{J}$ is evaluated. Against the warm wall, Γ_2 (in red), a solid box (in black Ω_s) connects the warm wall to the optimization domain. The rest of the volume is fluid (Ω_f). The design function ρ may not vary in $\Omega_f \cup \Omega_s$. Symmetry side, Γ_3: green contour.

In the present paper, we limit the study to heat sinks confined inside a three dimensional steady-state conductive differentially heated cavity, in which the buoyancy (under Boussinesq approximation) drives a swirling laminar convective flow.[14] We measure the enhancement of the heat sinks' thermal performance by evaluating the heat flux through the cold side of the cavity. For identifying the optimized design, the material distribution topology optimization method is combined with high-order accuracy steady-state direct numerical simulations (DNS) computed with the spectral element code `Nek5000`[15] and the `BoostConv` algorithm.[16] At each computational point in the domain, a material indicator function $\tilde{\rho}$ can describe the fluid ($\tilde{\rho} = 1$) or the solid ($\tilde{\rho} = 0$). The design function is allowed to attain values in the continuum $\tilde{\rho} \in [0, 1]$ in order to allow for gradient-based optimization algorithms. Penalty together with advanced filtering techniques[17] are employed in order to promote sharp interfaces and at the same time avoid small design features and mesh dependencies.

The paper is organized as follows. The problem is presented in Section 2 by outlining the governing equations and explaining how they are numerically solved. In Section 3 the filtering is described and in Section 4 the geometrical specification is given and the optimization algorithm is described. A thorough physical interpretation of the results

follows in Section 5, just before the conclusions.

2 PROBLEM PRESENTATION

The enhancement of the thermal performance of heat sinks is the primary focus of the present paper. We rely on the high-order accurate spectral element code `nek5000` together with a material-distribution topology optimization algorithm to numerically generate an effective geometry for a vertical heat sink enclosed in a conductive differentially heated cavity. The heat sink, attached to the warm wall of the cavity, is optimized for maximizing the heat transfer through the cavity, that is, the measure of the heat flux through the cold wall.

2.1 Physical specification

We describe the conjugate heat transfer problem originated by the interaction between an ideal Newtonian fluid and a solid structure. The incompressible flow under study is driven by natural convection (buoyancy force) and cools down the heat sink attached to the warm wall of the cavity. We limit the study to steady state conditions that are representative of a flow without instabilities and turbulence. We solve thus the steady state Navier–Stokes equations to evaluate the contribution of the thermal convection to the overall heat transfer, and we solve the energy conservation equation in the whole domain for computing the temperature distribution.

The chosen non-dimensionalization[18] relies on the Rayleigh and the Prandtl numbers

$$Ra = \frac{\rho^* C_f^* \beta^* |\mathbf{g}^*| \Delta T^* {x^*}^3}{\mu^* K_f^*}, \quad Pr = \frac{\mu^* C_f^*}{\rho^* k_f^*}, \tag{1}$$

respectively, in which the reference length, velocity, temperature, pressure, and time are

$$x^*_{\text{ref}} = L^*, \quad u^*_{\text{ref}} = \frac{k_f^* \sqrt{Ra}}{C_f^* L^*}, \quad \theta^*_{\text{ref}} = \Delta T^*, \quad p^*_{\text{ref}} = \rho^* {u^*_{\text{ref}}}^2 Pr, \quad t^*_{\text{ref}} = \frac{L^*}{u^*_{\text{ref}}}, \tag{2}$$

respectively. Additionally, k^* defines the thermal conductivity; C^* the thermal heat capacity (the subscript s and f indicate solid and fluid, respectively); ρ^*, μ^*, and β^* are the density, the viscosity, and the thermal expansion coefficient of the fluid, respectively. All dimensional variables are identified by a star, L^* is the cavity length, ΔT^* is the temperature difference with respect to the ambient, and $\mathbf{e}_g = -\mathbf{g}^*/|\mathbf{g}^*|$ is the unit gravity vector. As the dimensionless governing equations

$$\begin{aligned} \frac{1}{Pr}(\mathbf{u}\cdot\nabla)\mathbf{u} - \frac{1}{\sqrt{Ra}}\nabla^2\mathbf{u} + \nabla p - \mathbf{e}_g\theta + \chi(\tilde{\rho})\mathbf{u} &= 0, \\ C(\tilde{\rho})(\mathbf{u}\cdot\nabla)\theta - \frac{1}{\sqrt{Ra}}\nabla\cdot k(\tilde{\rho})\nabla\theta &= 0, \\ \nabla\cdot\mathbf{u} &= 0, \end{aligned} \tag{3}$$

show, under the Boussinesq approximation, the flow is driven by temperature variations. Moreover, we model the effect of the solid structure on the fluid flow as the action of a

Brinkman friction term[12] in the momentum equations. The amplitude of the Brinkman force $\chi(\tilde{\rho})$ has a direct dependence on the material indicator function $\tilde{\rho}$ that is continuously defined in the whole domain (solid: $\tilde{\rho} = 0$; fluid: $\tilde{\rho} = 1$). The function $\tilde{\rho}$ is, in turn, obtained from the design function ρ through the filtering operation described in Section 3. Also in the temperature equation, we rely on $\tilde{\rho}$ for defining its coefficients,[13] the adjusted non-dimensional heat capacity $C(\tilde{\rho})$ and the non-dimensional thermal conductivity $k(\tilde{\rho})$. The interpolation of the coefficients is done using *SIMP*-type functions:[2]

$$\chi(\tilde{\rho}) = \overline{\chi}(1-\tilde{\rho})^p, \quad C(\tilde{\rho}) = 1-(1-\tilde{\rho})^p, \quad k(\tilde{\rho}) = \left(\frac{k_s}{k_f} - 1\right)(1-\tilde{\rho})^p\,, \tag{4}$$

where p is the exponent that characterizes the steepness of the interpolation. The choice of having an adjusted thermal heat capacity legitimates the use of the Brinkman friction term. Indeed, when using an immersed boundary method (IBM), there is inevitably a small but nonzero velocity also in the solid.[11] Since our analysis focuses on heat transfer optimization, we set to zero the dimensionless heat capacity coefficient in the solid regions ($C(\tilde{\rho}) = 0$, when $\tilde{\rho} = 0$) to eliminate unrealistic convection contributions.

Finally, we want to measure the the efficiency of the optimized geometry in terms of heat transfer maximization through the cavity. The Fourier law indicates that $\Phi^* = -k^*\nabla^*\theta^*\cdot\mathbf{n}$ is the heat flux density through a surface. Here, k^* is the thermal conductivity and the unit normal vector $\mathbf{n}$ indicates the orientation of the surface. The non-dimensional heat flux is thus computed as $\Phi = k^*/k_f^*\nabla\theta\cdot\mathbf{n}$.

2.2 Numerical specification

To numerically solve the governing equations (3), we rely on the spectral-element solver `Nek5000`.[15] The code requires the computational domain to be divided in non-overlapping deformable quadrilaterals, in each of which a tensor product of Legendre polynomials of order N spans the solution. Additionally, the solution is required to satisfy a $\mathcal{C}^0$ continuity condition across the elements. At the N+1 Gauss–Lobatto–Legendre (GLL) quadrature nodes on each element, the velocity $\mathbf{u}$ and the temperature θ are evaluated with Lagrangian interpolants.[19] To guarantee skew symmetry of the advection term in the momentum conservation equations, over-integration is applied. Moreover, to suppress spurious pressure modes, the pressure p is evaluated as a Lagrangian interpolant of lower order $(N-2)$ on a staggered grid ($\mathbb{P}_N - \mathbb{P}_{N-2}$ method[20]).

Moreover, to compute the steady-state solution of the governing equations, a time marching scheme with enhanced convergence is used, the `BoostConv` method.[16] The algorithm treats the time evolution of Equation (3) as an iterative algorithm for solving general large-scale linear systems. A continuously adapting basis of size N is defined, which spans the $\mathbf{r}^n = [\mathbf{u};\theta]^{n+1} - [\mathbf{u};\theta]^n$ residuals in time. With this basis, a least-square problem is solved to obtain a modified residual ξ^n, which is used to recompute $[\mathbf{u};\theta]^{n+1} = [\mathbf{u};\theta]^n + \xi^n$and thus minimize the residual at iteration $n+1$.[21]

3 DESIGN DEFINITION

The material indicator function $\tilde{\rho}$, whose use has been described in Section 2.1, is defined indirectly through nonlinear filtering of an auxiliary design variable ρ. In particular, for the present study we have considered density filters to impose a length scale R to the optimized structures.[22,23] A cascade of so-called fW-mean nonlinear filters[17] is used to obtain an approximation of the so-called *open* operation from mathematical morphology.[24] We start by considering the classic linear filter[25] F_L, defined as the weighted convolution of two functions

$$F_L(\rho)(\mathbf{x}') = \frac{(\rho * \omega)(\mathbf{x}')}{W(\mathbf{x}')} = \frac{\int_\Omega \rho(\mathbf{x})\omega(|\mathbf{x}-\mathbf{x}'|)\,\mathrm{d}\mathbf{x}}{W(\mathbf{x}')}, \quad \text{where}$$
$$W(\mathbf{x}') = \int_\Omega \omega(|\mathbf{x}-\mathbf{x}'|)\,\mathrm{d}\mathbf{x}, \quad \omega = \begin{cases} \frac{2}{3}\left(\frac{3}{2}-|r|\right)^2 & \text{if} \quad \frac{1}{2} \le |r| \le \frac{3}{2} \\ 1-\frac{4}{3}|r|^2 & \text{if} \quad 0 \le |r| < \frac{1}{2} \end{cases}, \quad r = \frac{3}{2}\frac{|\mathbf{x}-\mathbf{x}'|}{R}. \tag{5}$$

To perform the open filter operation using fW-mean nonlinear filters, we use first a F_E *erode* operation, followed by a F_D *dilate* one,

$$F_E(\rho) = f_E^{-1} \circ \Big(F_L\big(f_E \circ \rho\big)\Big), \quad F_D(\rho) = f_D^{-1} \circ \Big(F_L\big(f_D \circ \rho\big)\Big), \tag{6}$$

where $\circ$ indicates a composition of two function, as $(f_E \circ \rho)(\mathbf{x}) = f_E(\rho(\mathbf{x}))$. The functions f_E and f_D, together with their inverse f_E^{-1} and f_D^{-1} are, for $s \in \Re$, defined as

$$f_E(s) = \frac{1}{s+\beta}, \quad f_D(s) = \frac{1}{1-s+\beta}, \quad f_E^{-1}(s) = \frac{1}{s} - \beta, \quad f_D^{-1}(s) = 1 - \frac{1}{s} + \beta, \tag{7}$$

respectively, with parameter $\beta > 0$. We define our composite nonlinear filter as

$$\tilde{\rho} = F(\rho) = F_D\big(F_E(\rho)\big); \tag{8}$$

that is, we first compute the composition of f_E with the design variable ρ, then we apply the linear filter F_L to the result, in order to obtain $\rho' = F_L(f_E \circ \rho)$. Successively, we compose the inverse function f_E^{-1} with ρ' to obtain $\rho'' = F_E(\rho)$, which is composed with f_D to become the input of a second linear filter operation F_L ($\rho''' = F_L\big(f_D \circ \rho''\big)$). At last, we compose the inverse function f_D^{-1} with ρ''' to obtain $\tilde{\rho} = F_D(\rho'')$.

4 SETUP PRESENTATION

We measure the enhanced performance of the optimized heat sink by evaluating the heat flux through the cold wall of the cavity (Γ_1), that is our objective function

$$\mathscr{J} = \int_{\Gamma_1} -\frac{k^*}{k_f^*}\nabla\theta \cdot \mathbf{n}\,\mathrm{d}\Gamma. \tag{9}$$

4.1 Geometry specification

We impose no slip boundary conditions on all external walls. For the temperature, we impose on the vertical walls uniform Dirichlet boundary conditions (cold $\theta = 0$ at $x = 0.5$, Γ_1, and $\theta = 1$ at $x = -0.5$, Γ_2). At $z = 0$ we define a symmetry plane, Γ_3. All other external walls are by definition conductive (*i.e.* a Dirichlet boundary condition with decreasing temperature $\theta = 0.5 - x$). The gravity acts in the negative vertical direction $(-y)$, and due to the buoyancy force, the horizontal temperature gradient imposed by the boundary conditions (along x) generates a clockwise flow rotation.

In order to obtain structures that act as heat sinks, we consider the optimization domain (Ω_O) to be a subset of the computational domain ($-0.46 \leq x \leq -0.25$, $-0.25 \leq y \leq 0.25$, and $-0.25 \leq z \leq 0$, see Fig. 1 for more details). Outside the optimization domain the design function ρ is forced to be solid in all the collocation points inside the black box located against the warm wall (Ω_s), and fluid everywhere else (Ω_f).

4.2 Optimization problem

We want to optimize $\rho \in \mathcal{A} = \{\rho \in L^\infty(\Omega) \mid 0 \leq \rho \leq 1,\ \rho|_{\Omega_s} \equiv 0,\ \rho|_{\Omega_f} \equiv 1\}$ for maximizing $\mathscr{J}$ (see Eq. (9)). The constraints are the governing equations (3), the filter operation (8), the boundary conditions, and the maximal amount of solid volume

$$
\begin{aligned}
\min_{\rho\in\mathcal{A}} \quad & -\mathscr{J}\,, \\
\text{s.t.} \quad & \frac{1}{Pr}(\mathbf{u}\cdot\nabla)\mathbf{u} - \frac{1}{\sqrt{Ra}}\nabla^2\mathbf{u} + \nabla p - \mathbf{e}_g\theta + \chi(\tilde{\rho})\mathbf{u} = 0 \ \text{ in } \Omega, \\
& C(\tilde{\rho})(\mathbf{u}\cdot\nabla)\theta - \frac{1}{\sqrt{Ra}}\nabla\cdot k(\tilde{\rho})\nabla\theta = 0 \ \text{ in } \Omega, \\
& \nabla\cdot\mathbf{u} = 0 \ \text{ in } \Omega, \\
& \tilde{\rho} - F(\rho) = 0 \ \text{ in } \Omega, \\
& \mathbf{u} = 0 \ \text{ on } \Gamma\setminus\Gamma_3, \qquad \nabla\mathbf{u}\cdot\mathbf{n} = 0 \ \text{ on } \Gamma_3, \\
& \theta = 0 \ \text{ on } \Gamma_1, \qquad \theta = 1 \ \text{ on } \Gamma_2, \\
& \nabla\theta\cdot\mathbf{n} = 0 \ \text{ on } \Gamma_3, \qquad \theta = 0.5 - x \ \text{ on } \Gamma\setminus(\Gamma_1\cup\Gamma_2\cup\Gamma_3), \\
& \int_\Omega (1-\tilde{\rho})\,\mathrm{d}\Omega \leq V_{\max}.
\end{aligned}
\tag{10}
$$

To solve (10), we rely on the optimization algorithm MMA[26] together with adjoint-based gradient calculations.[7]

In detail, we first define an initial design ρ and then iteratively solve the following algorithm until convergence:

- Compute $\tilde{\rho} = F(\rho)$ (Eq. 8);
- Map $\tilde{\rho}$ to the coefficients $k,\ C,\ \chi$ (Eq. 4);
- Solve the governing equations (Eq. 3);

- Solve the adjoint problem

$$\begin{aligned}
&\frac{1}{Pr}(-(\mathbf{u}\cdot\nabla\mathbf{u}^\dagger)+(\nabla\mathbf{u})^{\mathrm{T}}\cdot\mathbf{u}^\dagger)-\frac{1}{\sqrt{Ra}}\nabla^2\mathbf{u}^\dagger-\nabla p^\dagger+C(\nabla\theta)\theta^\dagger+\chi\mathbf{u}^\dagger=0,\\
&-\mathbf{e}_g\cdot\mathbf{u}^\dagger-C(\mathbf{u}\cdot\nabla)\theta^\dagger-\frac{1}{\sqrt{Ra}}\nabla\cdot k\nabla\theta^\dagger=0,\\
&\nabla\cdot\mathbf{u}^\dagger=0;\\
&\mathbf{u}^\dagger=0 \text{ on } \Gamma\setminus\Gamma_3, \qquad \nabla\mathbf{u}^\dagger\cdot\mathbf{n}=0 \text{ on } \Gamma_3,\\
&\theta^\dagger=\sqrt{Ra} \text{ on } \Gamma_2, \qquad \nabla\theta^\dagger\cdot\mathbf{n}=0 \text{ on } \Gamma_3, \qquad \theta^\dagger=0 \text{ on } \Gamma\setminus\Gamma_3\cup\Gamma_2,
\end{aligned} \tag{11}$$

- Compute the derivative of the objective function with respect to $\tilde{\rho}$:

$$\rho^\dagger=p(\tilde{\rho}-1)^{p-1}\theta^\dagger(\mathbf{u}\cdot\nabla)\theta+p(\frac{k_s}{k_f}-1)(1-\tilde{\rho})^{p-1}\frac{1}{\sqrt{Ra}}\nabla\theta^\dagger\cdot\nabla\theta+p\overline{\chi}(1-\tilde{\rho})^{p-1}\mathbf{u}^\dagger\cdot\mathbf{u}; \tag{12}$$

- Apply the following filter operation to obtain the function f

$$\begin{aligned}
f^\dagger(\mathbf{x}')&=\left(\int_\Omega\frac{\left(\rho^\dagger(\mathbf{x})\frac{1}{\rho''(\mathbf{x})^2}\right)\omega(|\mathbf{x}'-\mathbf{x}|)}{W(\mathbf{x})}\,\mathrm{d}\mathbf{x}\right)\frac{1}{(1-\rho''(\mathbf{x}')+\beta)^2},\\
f(\mathbf{x}')&=\left(\int_\Omega\frac{\left(f^\dagger(\mathbf{x})\frac{1}{\rho'(\mathbf{x})^2}\right)\omega(|\mathbf{x}'-\mathbf{x}|)}{W(\mathbf{x})}\,\mathrm{d}\mathbf{x}\right)\frac{1}{(\rho(\mathbf{x}')+\beta)^2},
\end{aligned} \tag{13}$$

  which contains the derivative of the objective function with respect to ρ;

- Use MMA to update ρ.

In brief, the fluid–thermal solver ensures that the governing equations and the boundary conditions are satisfied, whereas the MMA algorithm enforces the volume limitation and the conditions on ρ imposed by the definition of $\mathcal{A}$.

5 RESULTS

The optimization has been run for $Ra = 10^4$, using materials corresponding to air ($Pr = 0.71$) and aluminum ($k_s/k_f = 7749.1$). In the *SIMP* mapping (4), we have chosen $p = 5$, and for the filter a continuation technique on $\beta = \{1,\ 0.1\}$, $R = 0.02$. Based on a mesh independence study, the computational domain has been divided in 22 elements in x and y direction, 11 in the z direction, and with polynomial order 7 (about 10^4 degrees of freedom in the optimization domain). For the considered Ra, we have verified by computing the solution in the entire domain that the symmetry condition along z is not restricting the spectrum of optimal topologies. The results are shown in Figure 2. There, we can observe, from top to bottom, the optimized heat sinks (last column), which have been obtained starting with the initial designs shown in the first column, that is, uniform in Ω_O: $\rho = 0$, $\rho = 0.5$ (first two rows), and a classical vertical heat sink with

Table 1: Heat flux through Γ_1 with a uniform porous, a uniform solid initial design, and three vertical fins at the beginning of the optimization and at convergence.

	$\rho_0 = 0$	$\rho_0 = 0.5$	3 fins
$\mathscr{J}_0$	0.85	0.86	0.88
$\mathscr{J}_f$	0.93	0.93	0.92

three fins (last row), respectively. The structure is plotted with a gray iso-contour at $\tilde{\rho} = 0.5$ and the flow is represented by an iso-contour of velocity magnitude $|\mathbf{u}| = 0.19$ colored with the pseudo-colors of the temperature. With the same visual representation, we can observe in the central column of Figure 2, that the structure actively affects the flow. If we compare the flow before and after the optimization, then we notice that the fluid moving with $|\mathbf{u}| = 0.19$ is warmer. The overall velocity in the cavity increases, thus enhancing the convection contribution. Comparing the initial designs, from top to bottom, we can observe that a solid uniform medium inside Ω_O, creates an obstacle that strongly brakes the flow. The fluid accelerates vertically along the sides of the structure, and when it hits the top side of the cavity it decelerates at the expenses of the horizontal component of the velocity. Its contribution to the velocity magnitude along the top and bottom sides is substantially lower and therefore there are no $|\mathbf{u}| = 0.19$ flow structures at these locations. When we allow for some flow inside Ω_O, as in the case of uniform porous material and heat sink with three vertical fins, the velocity magnitude inside the cavity increases. Some $|\mathbf{u}| = 0.19$ flow structures appear along the top and bottom sides. They are better defined and of larger size for the heat sink that has a classical topology, since its geometry is designed to enhance the heat convection. Indeed, in Table 1 we can see that this configuration enhances the heat transfer, when compared to uniform material distributions inside Ω_O. However, it is not generally optimal for the flow under consideration. The vertical fins heat up the flows at x locations closer to the cold wall, similarly to the case with uniform solid Ω_O. Moreover, they are less invasive in the z direction and thus do not obstruct the flow as much as the solid block does. However, they do not optimize for the circulation. Therefore, to improve the circulation, the optimization carves the fins to create a double rake with larger harrows on the top sides and thinner elongated ones on the bottom sides. All optimized topologies can be considered similar; they enhance the convection contribution and induce a similar flow inside the cavity. The optimized structures canalize the fluid, increase the size of the higher speed flow structures, and modify their shape. The lower arms warm up the fluid at x locations further away from the warm wall, close to the limit of the optimization domain Ω_O. At these locations, the horizontal component of the velocity ($\mathbf{u}_x$) is higher, the structures create an obstacle that causes a bifurcation of the flow. Three main streams of warmer fluid flow upward, driven by buoyancy. We observe that the structure adapts its topology to canalize these streams to join again through the side holes. Additionally, with a smooth curved interface, which is divided in flat and shorter arms, it directs the flow towards the top-center of the cavity. This flow structures increase the thermal convection,

extract more heat from the heat sink and thus enhance the cooling performance of the solid structure (see Tab. 1). In the optimized geometry obtained starting from a vertical heat sink, the overall heat flux through Γ_1 is slightly lower. This is due to the more developed holes in the upper part of the structure, who allow for more vertical flow, therefore the maximal velocity magnitude is overall 3% lower.

6 CONCLUSIONS AND OUTLOOK

In the present paper, we successfully carried out topology optimization of heat sinks confined in a three dimensional differentially heated cavity. We base our results on the material distribution topology optimization method combined with high-order accuracy DNS combined with adjoint sensitivity analysis for the gradient computation. The flow is considered to be in steady-state, at laminar conditions ($Ra = 10^4$), and the cavity has conductive sides. The enhanced performances of the optimized structures are measured in terms of increase in the heat flux through the cold wall. For air ($Pr = 0.71$) and aluminum ($ks/kf = 7749.1$), the three scenarios considered are delivering an increase of the thermal performance of 8.5%, 7.3%,and 4.5% respectively. Advanced nonlinear filtering has been used to decouple the size of the smallest structure and the filter radius, as well as obtain sharp interfaces between fluid and solid material.[17] We deal with a nonlinear optimization problem, which is known for the presence of local optima and its dependency on the initial conditions. We, therefore, compare the results obtained for three different initial configurations and observe that the optimized geometries are different, but comparable in performance. They have common features, which act on the flow and thus optimize it for enhancing the thermal convection contribution. The optimized geometries are hollow in the center, have lower arms to bifurcate the warmer fluid, lateral holes for rejoining the warm streams flowing upward, and flat circular upper arms for smoothly directing the flow towards the center-top part of the cavity.

Further investigations will result in an extension of the present work. The impact of sizing parameters on the optimal topologies can be considered. In particular, it is of interest to see how different sizes of the optimization domain Ω_O, and of the sides of the cavity (*i.e.* aspect ratio $R = 4$ between the height and the other dimensions of the cavity) affect the final optimal design for the heat sink. In particular, in the last set of scenarios, not included in this paper, with an elongated cavity, the faster vertical flow, with a less rounded circulation, will have different topological requirements for enhancing the convection contribution.

Acknowledgments

The Swedish e-Science Research Center (SeRC) is acknowledged for funding this research. This research was also partially supported by the Swedish Foundation for Strategic Research (Grant No. AM13-0029). The computations were performed on resources provided by the Swedish National Infrastructure for Computing (SNIC) at the High Performance Computer Center North (HPC2N) at the Umeå University (UMU).

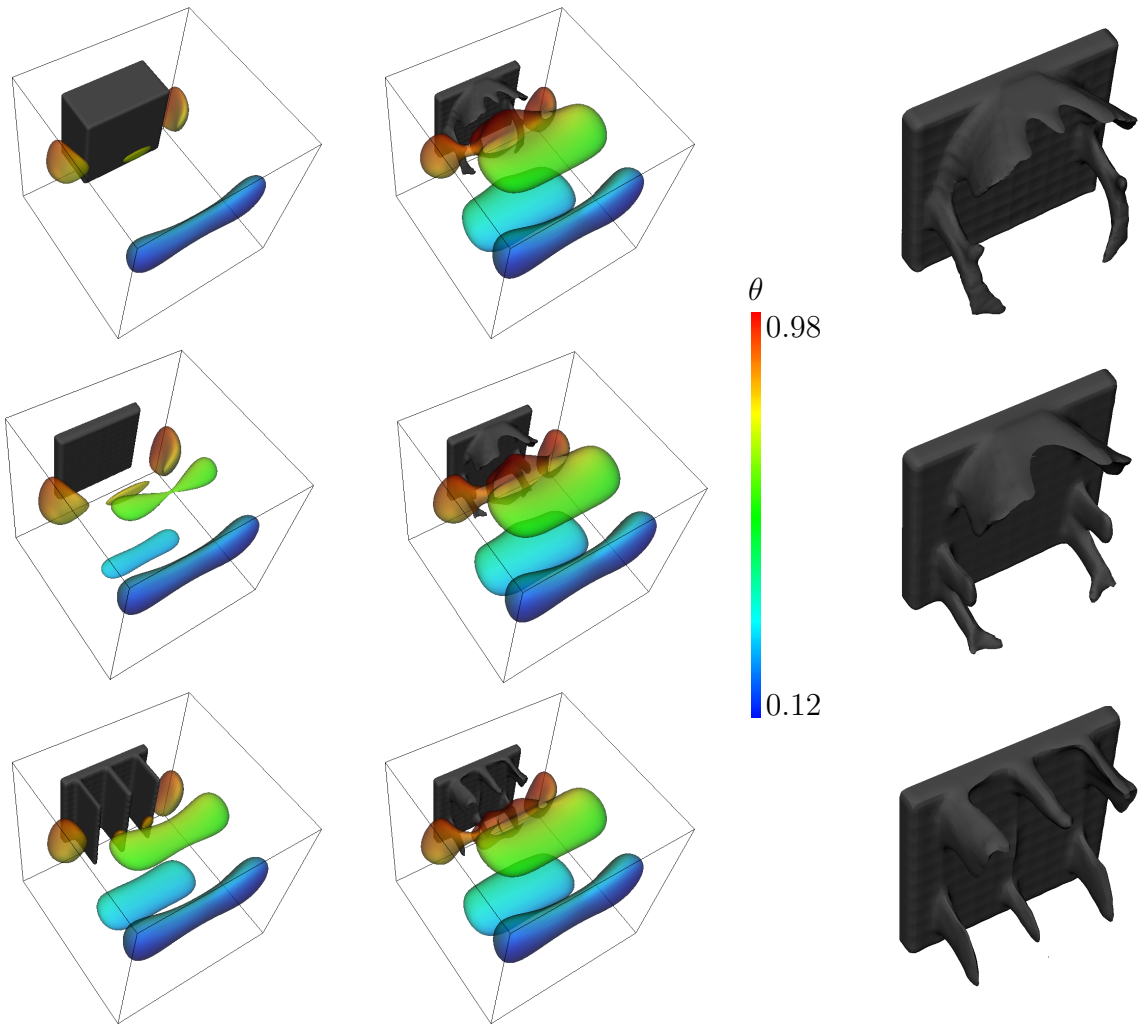

Figure 2: Optimized designs compared with the initial designs, from which they have been obtained. In gray, the structure (contour $\tilde{\rho} = 0.5$); with the pseudo-colors of the temperature θ, the flow structure represented by an iso-contour $|\mathbf{u}| = 0.19$. *Left:* Initial designs with surrounding flow. *Center:* Optimized topologies with surrounding flow. *Right:* Zoom on the optimal structures.

REFERENCES

[1] M.P. Bendsøe and N. Kikuchi. Generating optimal topologies in structural design using a homogenization method. *Computer Methods in Applied Mechanics and Engineering*, 71(2):197–224, 1988.

[2] M.P. Bendsøe and O. Sigmund. *Topology Optimization: Theory, Methods, and Applications*. Springer Berlin Heidelberg, thrird edition edition, 2011.

[3] T.E. Bruns. Topology optimization of convection-dominated, steady-state heat transfer problems. *International Journal of Heat and Mass Transfer*, 50:2859–2873, 2007.

[4] T. Borrvall and J. Petersson. Topology optimization of fluids in Stokes flow. *International Journal for Numerical Methods in Fluids*, 41(1):77–107, 2003.

[5] A.A. Koga, E.C.C. Lopes, H.F.V. Nova, C.R. De Lima, and E.C.N. Silva. Development of heat sink device by using topology optimization. *International Journal of Heat and Mass Transfer*, 64:759–772, 2013.

[6] J. Alexandersen, N. Aage, C.S. Andreasen, and O. Sigmund. Topology optimisation for natural convection problems. *International Journal for Numerical Methods in Fluids*, 76(10):699–721, 2014.

[7] C. Saglietti, P. Schlatter, E. Wadbro, M. Berggren, and D.S. Henningson. Topology optimization of heat sinks in a square differentially heated cavity. *Submitted*, 2018.

[8] J. Alexandersen, O. Sigmund, and N. Aage. Large scale three-dimensional topology optimisation of heat sinks cooled by natural convection. *International Journal of Heat and Mass Transfer*, 100:876–891, 2016.

[9] K. Yaji, T. Yamada, S. Kubo, K. Izui, and S. Nishiwaki. A topology optimization method for a coupled thermal–fluid problem using level set boundary expressions. *International Journal of Heat and Mass Transfer*, 81:878–888, 2015.

[10] C. H Villanueva and K. Maute. CutFEM topology optimization of 3d laminar incompressible flow problems. *Computer Methods in Applied Mechanics and Engineering*, 320:444–473, 2017.

[11] D. Goldstein, R. Handler, and L. Sirovich. Modeling a no-slip flow boundary with an external force field. *Journal of Computational Physics*, 105(2):354–366, 1993.

[12] H.C. Brinkman. A calculation of the viscous force exerted by a flowing fluid on a dense swarm of particles. *Flow, Turbulence and Combustion*, 1(1):27, 1949.

[13] T.E. Bruns. Topology optimization of convection-dominated, steady-state heat transfer problems. *International Journal of Heat and Mass Transfer*, 50(15):2859–2873, 2007.

[14] S. Xin and P. Le Quéré. Linear stability analyses of natural convection flows in a differentially heated square cavity with conducting horizontal walls. *Physics of Fluids*, 13(9):2529–2542, 2001.

[15] P.F. Fischer, J.W. Lottes, and S.G. Kerkemeier. Nek5000 web page. *Web page: http://nek5000. mcs. anl. gov*, 2008.

[16] V. Citro, P. Luchini, F. Giannetti, and F. Auteri. Efficient stabilization and acceleration of numerical simulation of fluid flows by residual recombination. *Journal of Computational Physics*, 344:234–246, 2017.

[17] L. Hägg and E. Wadbro. Nonlinear filters in topology optimization: existence of solutions and efficient implementation for minimum compliance problems. *Structural and Multidisciplinary Optimization*, 55(3):1017–1028, 2017.

[18] J.D. Hellums and S.W. Churchill. Transient and steady state, free and natural convection, numerical solutions: Part I. The isothermal, vertical plate. *AIChE Journal*, 8(5):690–692, 1962.

[19] M.O. Deville, P.F. Fischer, and E.H. Mund. *High-order Methods for Incompressible Fluid Flow*, volume 9. Cambridge university press, 2002.

[20] Y. Maday and A.T. Patera. Spectral element methods for the incompressible Navier-Stokes equations. In *IN: State-of-the-art surveys on computational mechanics (A90-47176 21-64).*, pages 71–143, 1989.

[21] M.A. Bucci. *Subcritical and Supercritical Dynamics of Incompressible Flow over Miniaturized Roughness Elements*. Phd thesis, École Nationale Supérieure d'Arts et Métiers, Paris, 2017.

[22] T. Borrvall. Topology optimization of elastic continua using restriction. *Archives of Computational Methods in Engineering*, 8(4):351–385, 2001.

[23] O. Sigmund. Morphology-based black and white filters for topology optimization. *Structural and Multidisciplinary Optimization*, 33(4):401–424, 2007.

[24] F. Y. Shih. *Image Processing and Mathematical Morphology: Fundamentals and Applications*. CRC press, 2009.

[25] T.E. Bruns and D.A. Tortorelli. Topology optimization of non-linear elastic structures and compliant mechanisms. *Computer Methods in Applied Mechanics and Engineering*, 190(26):3443–3459, 2001.

[26] K. Svanberg. The method of moving asymptotes a new method for structural optimization. *International Journal for Numerical Methods in Engineering*, 24(2):359–373, 1987.